5

Well Responses in Three-Zone Linear Composite Dual-Porosity Reservoirs

Jing-Jing Guo, Lie-Hui Zhang*, Hai-Tao Wang and Qi-Guo Liu
State Key Laboratory of Reservoir Geology and Exploitation,
Southwest Petroleum University
China

1. Introduction

Naturally fractured reservoirs are composed of high flow capacity-low storage fractures and high storage-low flow capacity matrix blocks. Composite systems in this type of reservoirs can be encountered as a result of non-uniform fracture distribution, drilling, secondary or tertiary recovery projects, and stimulation programs. In general, a composite reservoir system is made up of two or more regions. Each region has its own rock and fluid properties.

In the past 25 years, a considerable theoretical effort has been made to describe the pressure behavior of this specific type of reservoir. Poon (Poon, 1984) first studied the pressure transient behavior of a composite dual-porosity reservoir by extending the Warren and Root's natural fracture model to a composite reservoir and assuming pseudo-steady-state flow in the matrix system. In 1987, Prado and Da Prat (Prado & Da Prat, 1987) presented an analytical model to describe the pressure behavior of a well completed in a reservoir wherein natural fractures occur over a limited area around the wellbore. The flow in the reservoir is treated as a composite reservoir flow problem, the region adjacent to the wellbore being considered as a fractured medium and the outer region as a homogeneous one. Wellbore storage and skin effects were included in the solution, and the flow in the fractured region was mathematically described by Warren and Root's double porosity theory. In 1991, Satman (Satman, 1991) considered a model similar to Poon's but with transient interporosity flow. He presented the early- and late-time solutions in Laplace space but did not investigate the characteristics of the solution in dimensionless form. Kikani et al. (Kikani et al., 1991) and Olarewaju (Olarewaju, 1991) proposed an analytical model for naturally fractured reservoirs with transient interporosity flow and matrix skin in a composite reservoir.

In 1999, Guo & Xiang (Guo & Xiang, 1999) extended the radial composite dual-porosity model to multi-zone condition and put forward a well test model for a composite dual-porosity oil reservoir with non-uniform thickness and lateral heterogeneity. However, they did not give the analytical solution of the model. Based on the work done by Guo, Huang &

*Corresponding author

Liu (Huang & Liu, 2006) presented an analytical solution to describe the transient pressure behavior of a naturally fractured composite gas reservoir. More recently, the transient pressure distributions in dual-porosity composite reservoirs with different outer boundaries were discussed, considering variable rate (Huang et al., 2002; Li et al., 2007; Han et al., 2007; Zhang et al., 2010a, 2010b).

The mathematical models for radial composite dual-porosity reservoirs are well developed and validated by numerous studies. However, to our knowledge, the models for a well completed in a linear composite strip reservoir with natural fractures are poorly available in the literature. The effect of the formation thickness variation on the transient response of a well in this type of reservoir configuration also does not appear to have been considered previously in the literature.

In this chapter, based on the Warren and Root's natural fracture model, a new well test model for linear composite dual-porosity reservoirs is presented, considering formation thickness and reservoir properties variations in plane. The analytical solution is obtained with one finite Fourier cosine space transformation (Farlow, 1982) and time-space Laplace transformation. By using Duhamel principle, the corresponding wellbore pressure response, together with effects of skins and wellbore storage, is obtained. The type curves are plotted with Stehfest algorithm and the impacts of relevant parameters are discussed. The model as well as the method presented in this chapter is useful in predicting production performance or analyzing production data from this type of well-reservoir system.

2. Mathematical model

Our primary interest is to consider flow in a three-zone liner composite dual-porosity reservoir. In this section, we present the detailed derivation of the mathematical model.

2.1 Assumptions

The mathematical model proposed in this chapter is based on oil reservoir conditions; it is also applicable to gas reservoirs by replacing the pressure term with a pseudo-pressure term. The key assumptions made in developing the mathematical model include:

1. A dual-porosity strip reservoir with parallel impermeable boundaries can be divided into three regions. A constant-rate line-source well is located in region I as illustrated in Fig.1. The reservoir regions on both sides of the discontinuities may have different rock and fluid properties. But each one of the three zones is homogeneous and isotropic with constant reservoir properties such as permeability and porosity.
2. The matrix system is assumed to be a medium of high storativity and low permeability. It is also assumed that production is only by virtue of the fracture system; that is, the wellbore has no direct connection with the matrix system.
3. Single-phase slightly compressible fluid and isothermal flowing.
4. Reservoir properties change at the interface. Both the width and flow resistance along the interface are neglected.
5. Laminar flow in each zone, with negligible gravitational effect and capillary effect.
6. Uniform initial reservoir pressure (p_i).
7. Pseudo-steady-state interporosity flow.

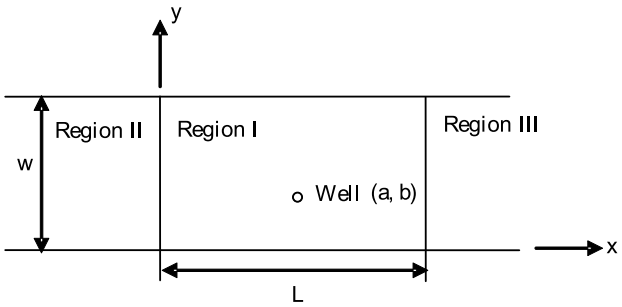

Fig. 1. Schematic of a three-zone linear composite dual-porosity reservoir

2.2 Definitions

Solutions in this chapter are presented in dimensionless form. Here, we first present the definitions of the dimensionless variables used in our derivation. All dimensionless variables are based on the properties of region I.

The dimensionless pressure for fracture system and the matrix system are defined respectively by

$$p_{Df} = \frac{2\pi k_{f1} h_1}{q\mu_1}\left(p_i - p_f\right) \tag{1}$$

$$p_{Dm} = \frac{2\pi k_{m1} h_1}{q\mu_1}\left(p_i - p_m\right) \tag{2}$$

The dimensionless time is defined by

$$t_D = \frac{k_{f1} t}{\left(\phi C_t\right)_{(f+m)1} \mu_1 r_w^2} \tag{3}$$

The dimensionless distances in the *x*- and *y*- directions are defined, respectively, by

$$x_D = \frac{x}{r_w} \tag{4}$$

$$y_D = \frac{\pi}{w_D}\frac{y}{r_w} \tag{5}$$

$$a_D = \frac{a}{r_w} \tag{6}$$

$$w_D = \frac{w}{r_w} \tag{7}$$

$$b_D = \frac{b}{r_w}\frac{\pi}{w_D} \tag{8}$$

The dimensionless variables related to the composite system are also defined in this section. The mobility ratios are defined by

$$M_{21} = \frac{k_{f2} / \mu_2}{k_{f1} / \mu_1} \tag{9}$$

and

$$M_{31} = \frac{k_{f3} / \mu_3}{k_{f1} / \mu_1} \tag{10}$$

The thickness ratios are defined as

$$h_{21} = \frac{h_2}{h_1} \tag{11}$$

and

$$h_{31} = \frac{h_3}{h_1} \tag{12}$$

The transmissibility ratios are defined as

$$\eta_{21} = \frac{k_{f2}/(\phi C_t)_{(f+m)2}\,\mu_2}{k_{f1}/(\phi C_t)_{(f+m)1}\,\mu_1} \tag{13}$$

and

$$\eta_{31} = \frac{k_{f3}/(\phi C_t)_{(f+m)3}\,\mu_3}{k_{f1}/(\phi C_t)_{(f+m)1}\,\mu_1} \tag{14}$$

As in the standard dual-porosity models, we also define the following dimensionless dual-porosity parameters. The storativity ratio is defined by

$$\omega_i = \frac{(\phi C_t)_{fi}}{(\phi C_t)_{(f+m)i}} \tag{15}$$

The interporosity flow coefficient is defined by

$$\lambda_i = \alpha \frac{k_{mi}}{k_{fi}} r_w^2 \tag{16}$$

where α is the interporosity shape factor and assumed to be identical for the three regions.

2.3 Fracture and matrix equations

Based on the assumptions and the coordinate system shown in Fig.1, the diffusivity equations governing the flow of a slightly compressible fluid in the fracture system of region I, region II and region III, respectively, are obtained by using the law of conservation of mass and are given by

$$-\nabla\cdot\left(\rho_1 v_{f1}\right)-\frac{q\delta(x-a)\delta(y-b)}{h_1}+q_1^*=\frac{\partial\left(\rho_1\phi_{f1}\right)}{\partial t}\ \text{ for }\ 0\le x\le L \tag{17}$$

$$-\nabla\cdot\left(\rho_2 v_{f2}\right)+q_2^*=\frac{\partial\left(\rho_2\phi_{f2}\right)}{\partial t}\ \text{ for }\ x\le 0 \tag{18}$$

$$-\nabla\cdot\left(\rho_3 v_{f3}\right)+q_3^*=\frac{\partial\left(\rho_3\phi_{f3}\right)}{\partial t}\ \text{ for }\ x\ge L \tag{19}$$

We now assume that Darcy's Law holds. We restrict our attention to Newtonian fluids and isothermal conditions. In this chapter, we restrict our attention to the isotropy case. Thus, the velocity of the fluid is given by

$$v_{fi}=-\frac{k_{fi}}{\mu_i}\nabla p_{fi}\quad i=1,2,3 \tag{20}$$

where the subscripts 1, 2 and 3 refer to regions I, region II and region III.

The total isothermal compressibility of the fracture system in region *i* is given by

$$C_{tfi}=\left(\frac{1}{\rho_i}\frac{\partial\rho_i}{\partial p_{fi}}\right)_{T=const}+\left(\frac{1}{\phi_i}\frac{\partial\phi_i}{\partial p_{fi}}\right)_{T=const}\quad i=1,2,3 \tag{21}$$

Insertions of the expressions on the right-hand sides of Eqs. (20) and (21) for the appropriate expressions in Eqs. (17) to (19) yield the following diffusion equations

$$\frac{\partial^2 p_{f1}}{\partial x^2}+\frac{\partial^2 p_{f1}}{\partial y^2}-\frac{q\mu_1\delta(x-a)\delta(y-b)}{k_{f1}h_1}+q_1^*=\frac{\left(\phi_f\mu C_{tf}\right)_1}{k_{f1}}\frac{\partial p_{f1}}{\partial t}\ \text{ for }\ 0\le x\le L \tag{22}$$

$$\frac{\partial^2 p_{f2}}{\partial x^2}+\frac{\partial^2 p_{f2}}{\partial y^2}+q_2^*=\frac{\left(\phi_f\mu C_{tf}\right)_2}{k_{f2}}\frac{\partial p_{f2}}{\partial t}\ \text{ for }\ x\le 0 \tag{23}$$

$$\frac{\partial^2 p_{f3}}{\partial x^2}+\frac{\partial^2 p_{f3}}{\partial y^2}+q_3^*=\frac{\left(\phi_f\mu C_{tf}\right)_3}{k_{f3}}\frac{\partial p_{f3}}{\partial t}\ \text{ for }\ x\ge L \tag{24}$$

where δ is the delta function denoting the constant-rate line-source well, and q^* is the volumetric flow rate from the matrix system to the fracture system.

Ignoring flow within the matrix system, the diffusivity equations for the matrix system of region I, region II and region III, are given by

$$\left(\phi_m C_{tm}\right)_1 \frac{\partial p_{m1}}{\partial t} + q_1^* = 0 \text{ for } 0 \le x \le L \tag{25}$$

$$\left(\phi_m C_{tm}\right)_2 \frac{\partial p_{m2}}{\partial t} + q_2^* = 0 \text{ for } x \le 0 \tag{26}$$

$$\left(\phi_m C_{tm}\right)_3 \frac{\partial p_{m3}}{\partial t} + q_3^* = 0 \text{ for } x \ge L \tag{27}$$

Flow from the matrix system to the fracture system is proportional to the difference between the pressures of the two systems. If we assume pseudosteady flow from the matrix system to the fracture system (Warren and Root idealization), then we can also write

$$q_1^* = \alpha \frac{k_{m1}}{k_{f1}}\left(p_{m1} - p_{f1}\right) \tag{28}$$

$$q_2^* = \alpha \frac{k_{m2}}{k_{f2}}\left(p_{m2} - p_{f2}\right) \tag{29}$$

$$q_3^* = \alpha \frac{k_{m3}}{k_{f3}}\left(p_{m3} - p_{f3}\right) \tag{30}$$

Combining Eqs. (22) to (30), the following equations are obtained.

$$\frac{\partial^2 p_{f1}}{\partial x^2} + \frac{\partial^2 p_{f1}}{\partial y^2} - \frac{q\mu_1 \delta(x-a)\delta(y-b)}{k_{f1} h_1} + \alpha \frac{k_{m1}}{k_{f1}}\left(p_{m1} - p_{f1}\right) = \frac{\left(\phi_f \mu C_{tf}\right)_1}{k_{f1}} \frac{\partial p_{f1}}{\partial t}$$

$$\text{for } 0 \le x \le L \tag{31}$$

$$\left(\phi_m C_{tm}\right)_1 \frac{\partial p_{m1}}{\partial t} + \alpha \frac{k_{m1}}{\mu_1}\left(p_{m1} - p_{f1}\right) = 0 \text{ for } 0 \le x \le L \tag{32}$$

$$\frac{\partial^2 p_{f2}}{\partial x^2} + \frac{\partial^2 p_{f2}}{\partial y^2} + \alpha \frac{k_{m2}}{k_{f2}}\left(p_{m2} - p_{f2}\right) = \frac{\left(\phi_f \mu C_{tf}\right)_2}{k_{f2}} \frac{\partial p_{f2}}{\partial t} \text{ for } x \le 0 \tag{33}$$

$$\left(\phi_m C_{tm}\right)_2 \frac{\partial p_{m2}}{\partial t} + \alpha \frac{k_{m2}}{\mu_2}\left(p_{m2} - p_{f2}\right) = 0 \text{ for } x \le 0 \tag{34}$$

$$\frac{\partial^2 p_{f3}}{\partial x^2} + \frac{\partial^2 p_{f3}}{\partial y^2} + \alpha \frac{k_{m3}}{k_{f3}}\left(p_{m3} - p_{f3}\right) = \frac{\left(\phi_f \mu C_{tf}\right)_3}{k_{f3}} \frac{\partial p_{f3}}{\partial t} \text{ for } x \ge L \tag{35}$$

$$(\phi_m C_{tm})_3 \frac{\partial p_{m3}}{\partial t} + \alpha \frac{k_{m3}}{\mu_3}\left(p_{m3} - p_{f3}\right) = 0 \text{ for } x \geq L \tag{36}$$

Based on the definitions of dimensionless variables, Eqs. (31) to (36) can be written as

$$\frac{\partial^2 p_{Df1}}{\partial x_D^2} + \left(\frac{\pi}{w_D}\right)^2 \frac{\partial^2 p_{Df1}}{\partial y_D^2} + \frac{2\pi^2 \delta(x_D - a_D)\delta(y_D - b_D)}{w_D} = \omega_1 \frac{\partial p_{Df1}}{\partial t_D} - \lambda_1 \left(\frac{k_{f1}}{k_{m1}} p_{Dm1} - p_{Df1}\right)$$

$$\text{for } 0 \leq x_D \leq L_D \tag{37}$$

$$\lambda_1 \left(p_{Dm1} - \frac{k_{m1}}{k_{f1}} p_{Df1}\right) + (1 - \omega_1) \frac{\partial p_{Dm1}}{\partial t_D} = 0 \text{ for } 0 \leq x_D \leq L_D \tag{38}$$

$$\frac{\partial^2 p_{Df2}}{\partial x_D^2} + \left(\frac{\pi}{w_D}\right)^2 \frac{\partial^2 p_{Df2}}{\partial y_D^2} + \lambda_2 \left(\frac{k_{f1}}{k_{m1}} p_{Dm2} - p_{Df2}\right) = \frac{\omega_2}{\eta_{21}} \frac{\partial p_{Df2}}{\partial t_D} \text{ for } x_D \leq 0 \tag{39}$$

$$\lambda_2 \eta_{21} \left(p_{Dm2} - \frac{k_{m1}}{k_{f1}} p_{Df2}\right) + (1 - \omega_2) \frac{\partial p_{Dm2}}{\partial t_D} = 0 \text{ for } x_D \leq 0 \tag{40}$$

$$\frac{\partial^2 p_{Df3}}{\partial x_D^2} + \left(\frac{\pi}{w_D}\right)^2 \frac{\partial^2 p_{Df3}}{\partial y_D^2} + \lambda_3 \left(\frac{k_{f1}}{k_{m1}} p_{Dm3} - p_{Df3}\right) = \frac{\omega_3}{\eta_{31}} \frac{\partial p_{Df3}}{\partial t_D} \text{ for } x_D \geq L_D \tag{41}$$

$$\lambda_3 \eta_{31} \left(p_{Dm3} - \frac{k_{m1}}{k_{f1}} p_{Df3}\right) + (1 - \omega_3) \frac{\partial p_{Dm3}}{\partial t_D} = 0 \text{ for } x_D \geq L_D \tag{42}$$

The initial conditions can be described as

$$p_{Df1}\big|_{t_D=0} = p_{Df2}\big|_{t_D=0} = p_{Df3}\big|_{t_D=0} = 0 \tag{43}$$

and

$$p_{Dm1}\big|_{t_D=0} = p_{Dm2}\big|_{t_D=0} = p_{Dm3}\big|_{t_D=0} = 0 \tag{44}$$

The outer boundary conditions in x direction are

$$\lim_{x_D \to -\infty} p_{Df2} = 0 \tag{45}$$

and

$$\lim_{x_D \to \infty} p_{Df3} = 0 \tag{46}$$

The outer boundary conditions in y direction are

$$\left.\frac{\partial p_{Df1}}{\partial y_D}\right|_{y_D=\pi} = \left.\frac{\partial p_{Df1}}{\partial y_D}\right|_{y_D=0} = 0 \tag{47}$$

$$\left.\frac{\partial p_{Df2}}{\partial y_D}\right|_{y_D=\pi} = \left.\frac{\partial p_{Df2}}{\partial y_D}\right|_{y_D=0} = 0 \tag{48}$$

and

$$\left.\frac{\partial p_{Df3}}{\partial y_D}\right|_{y_D=\pi} = \left.\frac{\partial p_{Df3}}{\partial y_D}\right|_{y_D=0} = 0 \tag{49}$$

The pressure continuities at the interface state

$$p_{Df1}\Big|_{x_D=0} = p_{Df2}\Big|_{x_D=0} \tag{50}$$

and

$$p_{Df1}\Big|_{x_D=L_D} = p_{Df3}\Big|_{x_D=L_D} \tag{51}$$

By using the law of conservation of mass, the flow continuities at the interface satisfy

$$\left.\frac{\partial p_{Df1}}{\partial x_D}\right|_{x_D=0} = M_{21}h_{21}\left.\frac{\partial p_{Df2}}{\partial x_D}\right|_{x_D=0} \tag{52}$$

$$\left.\frac{\partial p_{Df1}}{\partial x_D}\right|_{x_D=L_D} = M_{31}h_{31}\left.\frac{\partial p_{Df3}}{\partial x_D}\right|_{x_D=L_D} \tag{53}$$

3. Model solution

The finite Fourier cosine transformation and Laplace transformation are employed to solve the dimensionless well testing model.

The finite Fourier cosine transformation is defined as (Farlow, 1982)

$$\hat{G}(m) = C_m = F\left[G(y)\right] = \int_0^{\pi} G(y)\cos(my)dy \tag{54}$$

where m is the Fourier variable with respect to y_D. The inverse Fourier cosine transformation is defined as

$$G(y) = F^{-1}\left[\hat{G}(m)\right] = \frac{C_0}{\pi} + \frac{2}{\pi}\sum_{m=1}^{\infty} C_m \cos(my) \tag{55}$$

The Laplace transformation is defined as

$$\overline{F}(u) = L\left[F(t)\right] = \int_0^{+\infty} F(t)e^{-ut}dt \tag{56}$$

where u is the Laplace variable with respect to time.

With Eqs. (43) and (48), the Laplace transformation with respect to t_D and the finite Fourier cosine transformation with respect to y_D of Eqs. (39) and (40) yield

$$\frac{d^2\hat{\bar{p}}_{Df2}}{dx_D^2} - \alpha_2\hat{\bar{p}}_{Df2} = 0 \text{ for } x_D \le 0 \tag{57}$$

where $\alpha_2 = \left(\frac{m\pi}{w_D}\right)^2 + \frac{u\omega_2}{\eta_{21}} + \frac{\lambda_2 u(1-\omega_2)}{\lambda_2\eta_{21} + u(1-\omega_2)}$, $\hat{\bar{p}}_{Df2}$ is the dimensionless fracture pressure of region II in Fourier-Laplace space.

The solution to Eq. (57) with the outer boundary condition at $x_D \to -\infty$ is

$$\hat{\bar{p}}_{Df2} = Ae^{\sqrt{\alpha_2}x_D} \text{ for } x_D \le 0 \tag{58}$$

With Eqs. (43) and (49), the Laplace transformation with respect to t_D and the finite Fourier cosine transformation with respect to y_D of Eqs. (41) and (42) yield

$$\frac{d^2\hat{\bar{p}}_{Df3}}{dx_D^2} - \alpha_4\hat{\bar{p}}_{Df3} = 0 \text{ for } x_D \ge L_D \tag{59}$$

where $\alpha_4 = \left(\frac{m\pi}{w_D}\right)^2 + \frac{u\omega_3}{\eta_{31}} + \frac{\lambda_3 u(1-\omega_3)}{\lambda_3\eta_{31} + u(1-\omega_3)}$, $\hat{\bar{p}}_{Df3}$ is the dimensionless fracture pressure of region III in Fourier-Laplace space.

The solution to Eq. (59) with the outer boundary condition at $x_D \to \infty$ is

$$\hat{\bar{p}}_{Df3} = De^{-\sqrt{\alpha_4}x_D} \text{ for } x_D \ge L_D \tag{60}$$

With Eqs. (43) and (47), the Laplace transformation with respect to t_D and the finite Fourier cosine transformation with respect to y_D of Eqs. (37) and (38) yield

$$\frac{d^2\hat{\bar{p}}_{Df1}}{dx_D^2} - \alpha_1\hat{\bar{p}}_{Df1} = \alpha_3\delta(x_D - a_D) \text{ for } 0 \le x_D \le L_D \tag{61}$$

where $\alpha_1 = \left(\frac{m\pi}{w_D}\right)^2 + u\omega_1 + \frac{\lambda_1 u(1-\omega_1)}{\lambda_1 + u(1-\omega_1)}$, $\alpha_3 = -\frac{2\pi^2\cos(mb_D)}{uw_D}$, $\hat{\bar{p}}_{Df1}$ is the dimensionless fracture pressure of region I in Fourier-Laplace space.

The solution of Eq. (61) is not readily accessible because of the delta function at the right hand side. The Laplace transformation of Eq. (61) with respect to x_D yields

$$s^2 W_1 - s\hat{\bar{p}}_{Df1}(x_D=0) - \frac{\partial \hat{\bar{p}}_{Df1}}{\partial x_D}(x_D=0) - \alpha_1 W_1 = \alpha_3 e^{-a_D s} \tag{62}$$

where s is the Laplace variable with respect to x_D, and W_1 refers to $\hat{\bar{p}}_{Df1}$ in Laplace space with respect to x_D. Rearranging Eq. (62) and solving for W_1 yields

$$W_1 = \frac{\alpha_3 e^{-a_D s} + \frac{\partial \hat{\bar{p}}_{Df1}}{\partial x_D}(x_D=0) + s\hat{\bar{p}}_{Df1}(x_D=0)}{s^2 - \alpha_1} \tag{63}$$

A term-by-term Laplace inversion transformation and using conditions at the interface, yields

$$\hat{\bar{p}}_{Df1}(x_D,m,u) = A\frac{e^{\sqrt{\alpha_1}x_D} + e^{-\sqrt{\alpha_1}x_D}}{2} + \frac{AM_{21}h_{21}\sqrt{\alpha_2}}{\sqrt{\alpha_1}}\frac{e^{\sqrt{\alpha_1}x_D} - e^{-\sqrt{\alpha_1}x_D}}{2} \quad \text{for } 0 \le x_D \le a_D \tag{64}$$

and

$$\begin{aligned}&\hat{\bar{p}}_{Df1}(x_D,m,u)\\ &= \frac{\alpha_3}{\sqrt{\alpha_1}}\frac{e^{\sqrt{\alpha_1}(x_D-a_D)} - e^{-\sqrt{\alpha_1}(x_D-a_D)}}{2} + A\frac{e^{\sqrt{\alpha_1}x_D} + e^{-\sqrt{\alpha_1}x_D}}{2} + \frac{AM_{21}h_{21}\sqrt{\alpha_2}}{\sqrt{\alpha_1}}\frac{e^{\sqrt{\alpha_1}x_D} - e^{-\sqrt{\alpha_1}x_D}}{2}\\ &\qquad \text{for } a_D \le x_D \le L_D\end{aligned} \tag{65}$$

With Heaviside unit step function, Eqs. (64) and (65) can be rearranged as

$$\begin{aligned}&\hat{\bar{p}}_{Df1}(x_D,m,u)\\ &= \frac{\alpha_3}{\sqrt{\alpha_1}}\frac{e^{\sqrt{\alpha_1}(x_D-a_D)} - e^{-\sqrt{\alpha_1}(x_D-a_D)}}{2}H(x_D-a_D) \qquad \text{for } 0 \le x_D \le L_D\\ &+A\frac{e^{\sqrt{\alpha_1}x_D} + e^{-\sqrt{\alpha_1}x_D}}{2} + \frac{AM_{21}h_{21}\sqrt{\alpha_2}}{\sqrt{\alpha_1}}\frac{e^{\sqrt{\alpha_1}x_D} - e^{-\sqrt{\alpha_1}x_D}}{2}\end{aligned} \tag{66}$$

With Eq. (51) and Eq. (53), Eq. (66) yields

$$\begin{aligned}&\hat{\bar{p}}_{Df1}(x_D,m,u)\\ &= \frac{\alpha_3}{2\sqrt{\alpha_1}}\left[e^{\sqrt{\alpha_1}(x_D-a_D)} - e^{-\sqrt{\alpha_1}(x_D-a_D)}\right]H(x_D-a_D)\\ &+\frac{\alpha_3}{2\sqrt{\alpha_1}}\frac{ge^{\sqrt{\alpha_1}(x_D-2L_D+a_D)} - e^{\sqrt{\alpha_1}(x_D-a_D)} + fge^{-\sqrt{\alpha_1}(x_D+2L_D-a_D)} - fe^{-\sqrt{\alpha_1}(x_D+a_D)}}{1+fge^{-2\sqrt{\alpha_1}L_D}}\end{aligned}$$

$$\text{for } 0 \le x_D \le L_D \tag{67}$$

where $f = \dfrac{\sqrt{\alpha_1} - M_{21}h_{21}\sqrt{\alpha_2}}{\sqrt{\alpha_1} + M_{21}h_{21}\sqrt{\alpha_2}}$, $g = \dfrac{M_{31}h_{31}\sqrt{\alpha_4} - \sqrt{\alpha_1}}{M_{31}h_{31}\sqrt{\alpha_4} + \sqrt{\alpha_1}}$.

Eq. (67) is of an exponential form in the x_D variable, and the Laplace time variable and the Fourier y_D variable are in the α terms as described above. This is a general solution that gives the pressure response at any point in the reservoir. It can be used to compute the response at the wellbore, which is done in this chapter. The dimensionless wellbore pressure drawdown then can be calculated by setting x_D=a_D-1 and y_D=b_D in Eq. (67), that is

$$\hat{\bar{p}}^{*}_{wfD}(m,u) = \frac{\alpha_3}{2\sqrt{\alpha_1}} \frac{ge^{\sqrt{\alpha_1}(2a_D - 2L_D - 1)} - e^{-\sqrt{\alpha_1}} + fge^{-\sqrt{\alpha_1}(2L_D - 1)} - fe^{\sqrt{\alpha_1}}}{1 + fge^{-2\sqrt{\alpha_1}L_D}} \tag{68}$$

The wellbore storage and skin are not included in the dimensionless wellbore pressure calculated by the above equation.

4. Computational considerations

In the preceding sections, we have developed a solution for a well in a three-zone linear composite dual-porosity reservoir. In fact, obtaining the solution for the pressure distribution is only the first step toward the computation of well responses. The major contribution of this section is to provide the means to compute the solution presented in the preceding sections.

4.1 Wellbore storage

When a well is opened, the production at surface is initially due to the expansion of the fluid stored in the wellbore, and the reservoir contribution is initially negligible. This characteristic flow regime, called the pure wellbore storage effect, can last from a few seconds to a few minutes. Then, the reservoir production starts and the sand face rate increases until it becomes the same as the surface rate. When this condition is reached, the wellbore storage has no effect any more on the bottom hole pressure response, the data describes the reservoir behavior and it can be used for transient analysis.

After any change in the well flowing conditions, there is a time lag between the surface production and the sand face rate. The effect of wellbore storage affects well pressure responses during the first instants of each test period. In this chapter, only drawdown responses are illustrated. The wellbore storage coefficient C is used to describe this process (Bourdet, 2000).

4.2 Skin

For a damaged well, an additional pressure drop Δp_s is present when the reservoir fluid enters into the well. The magnitude of Δp_s reflect the extent of reservoir damage. However, the same Δp_s can describe a low or very high damage, depending on the flow rate and the

reservoir property. For comparison between different wells, the magnitude of the pressure drop near the wellbore has to be normalized. The skin factor S, a dimensionless parameter, is introduced to normalize the pressure drop.

The wellbore pressure with effects of wellbore storage and skins in Laplace space is calculated by using Duhamel principle expressed by the following equation

$$\hat{\bar{p}}_{wfD} = \frac{u\hat{\bar{p}}^{*}_{wfD} + S}{u\left[1 + uC_D\left(u\hat{\bar{p}}^{*}_{wfD} + S\right)\right]} \tag{69}$$

where C_D is the dimensionless wellbore storage coefficient, $\hat{\bar{p}}^{*}_{wfD}$ is the dimensionless wellbore pressure drop with zero skin and wellbore storage in Laplace-Fourier space, which is calculated by Eq. (69). And $\hat{\bar{p}}_{wfD}$ is the dimensionless wellbore pressure drop incorporating wellbroe storage and skin in Laplace-Fourier space.

4.3 Finite Fourier transformation inversion

The solution presented in the preceding section is in the Laplace-Fourier domain. To obtain the wellbore pressure response in real space, an accurate Fourier inversion is needed. The Fourier cosine transformation used in this chapter is inverted numerically with Eq. (55). The convergence in numerical inversion of the Fourier transformation is assumed to be reached if the absolute value of the ratio of the sum of the m, m-1 and m-2 terms in Eq. (55) to the total sum is less than 10^{-14}. In some cases, the solution converges extremely slowly – in fact, for certain time ranges the series behave as if it is a divergent. More than 1000 terms in Eq. (55) are required at early time to achieve convergence.

4.4 Laplace transformation inversion

The Stehfest algorithm is used to invert the Laplace transformation numerically. The fundamental principle of Stehfest algorithm is given by

$$p_{wfD}\left(t_D\right) = \frac{\ln 2}{t_D}\sum_{i=1}^{N} V\left(i\right)\bar{p}_{wfD}\left[s\left(i\right)\right] \tag{70}$$

where

$$s\left(i\right) = \frac{\ln 2}{t_D} i \tag{71}$$

$$V\left(i\right) = \left(-1\right)^{\frac{N}{2}+i} \sum_{k=\left\lfloor\frac{i+1}{2}\right\rfloor}^{\min\left\{\frac{N}{2},i\right\}} \frac{k^{\frac{N}{2}+1}\left(2k\right)!}{\left(\frac{N}{2}-k\right)!\left(k!\right)^2\left(i-k\right)!\left(2k-i\right)!} \tag{72}$$

At this point, a remark on the use of the Stehfest algorithm appears to be appropriate. The accuracy of the results obtained by using the numerical inversion algorithm suggested by

Stehfest is governed by a parameter denoted by N. Briefly, the parameter N determines the number of terms to be considered in the computation of the series used to approximate the Laplace inversion of the subject function. Theoretically, the accuracy of the numerical inversion should improve as the value of N increases. In practice, however, as N becomes too large, the result suffers from rounding errors. In this chapter, the inversion of the Laplace transformation is performed using Stehfest algorithm, with n=6. This allows us to relax the convergence criteria, because for n=8 or n=10, the inverse Fourier transform would be longer to compute, as Stehfest algorithm would require a higher precision.

5. Type curves and discussions

The pressure-transient behavior of a well in a three-zone linear composite dual-porosity reservoir with varied thickness and lateral heterogeneity is presented in this section. The steps to generate the type curves are as follows

1. The finite Fourier cosine transformation is inverted numerically.
2. The Laplace transformation is inverted numerically by Stehfest algorithm.
3. Calculate the wellbore pressure responses in real space.
4. Plot the type curves (log-log graph of pressure and derivative) based on the results obtained from the steps above.

The characteristics of type curves and the effects of correlating parameters are presented as follows. It is recognized that there are a number of variables which may affect the characteristics of type curves, such as thickness ratio, mobility ratio, transmissibility ratio, well location in the reservoir (a_D and b_D) and reservoir width w_D. The effects of all these parameters on type curves are discussed in detailed in this chapter.

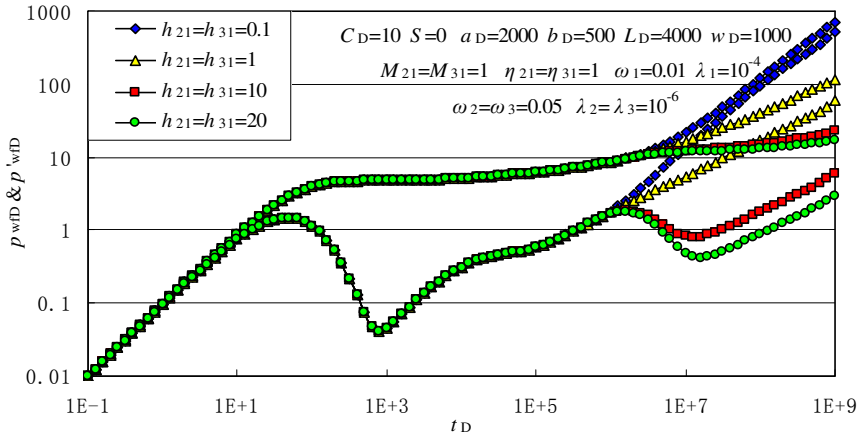

Fig. 2. Effect of thickness ratio on pressure responses for a well in a three-zone linear composite dual-porosity reservoir ($h_{21}=h_{31}$)

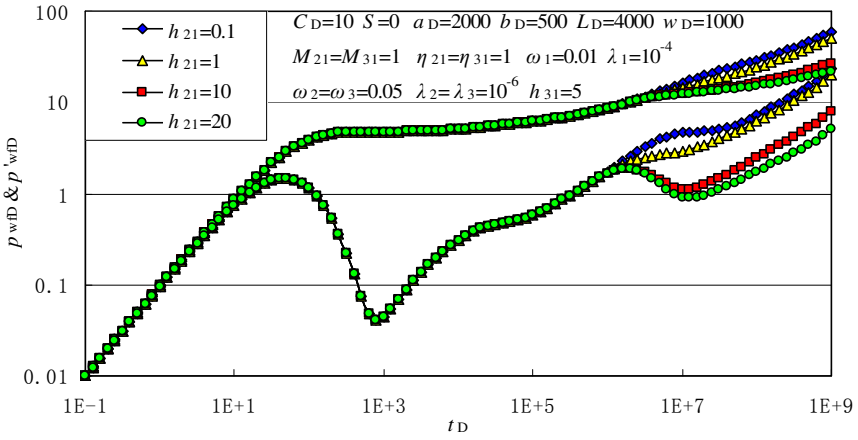

Fig. 3. Effect of thickness ratio on pressure responses for a well in a three-zone linear composite dual-porosity reservoir (h_{21}≠h_{31})

Figs.2 and 3 depict the pressure responses as a result of varied thickness ratios. Wellbore storage period, interporosity flow period and total radial flow period in region I can be observed from all the two figures. The effect of thickness ratio on type curves becomes obvious after the pressure wave reaches the interface.

It is can be seen that because the parallel impermeable boundaries are closer to the well than the facies changes, thus the derivative first displays the 1/2 slope characteristic of linear flow. Before the pressure wave reaches the interface, the wellbore pressure drawdown merely depends on reservoir properties of region I and has nothing to do with thickness ratio. Once the pressure wave reaches the interface, the following pressure behavior then is the result of average reservoir values of region I, region II and region III.

For the case the thickness ratio bigger than unit, after the pressure wave reaching the interface, the average flow capacity improves and the pressure drop consumed in fluid flow in reservoir decreases, the elevations of dimensionless pressure and pressure derivative curves get lower. The greater the thickness ratio is, the lower the pressure and pressure derivative curves are. Whereas if the thickness ratio is smaller than unit, after the pressure wave reaching the interface, the average flow capacity recedes and the pressure drop consumed in fluid flow in reservoir increases, the elevations of dimensionless pressure and pressure derivative curves get higher. The smaller the thickness ratio is, the higher the pressure and pressure derivative curves are.

In addition, Fig.2 also presents the limiting case that when the thickness of outer region (i.e. region II and III) is small enough, the derivative finally displays a unit slope instead of a 1/2 slope which is the characteristic of a closed system.

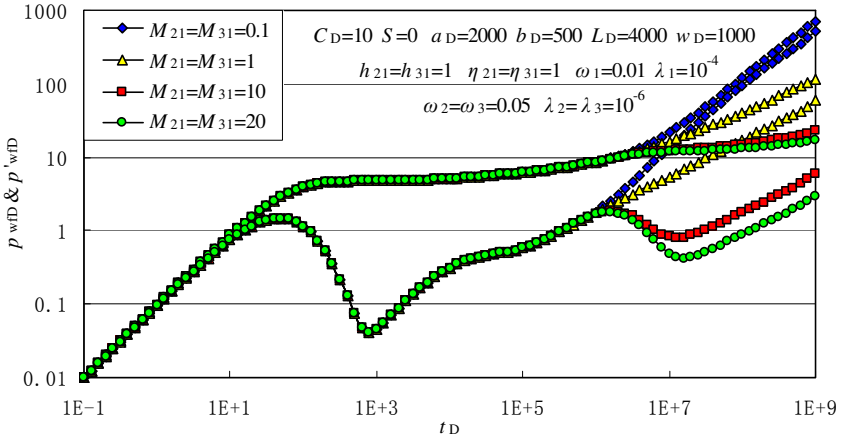

Fig. 4. Effect of mobility ratio on pressure responses for a well in a three-zone linear composite dual-porosity reservoir (M_{21}=M_{31})

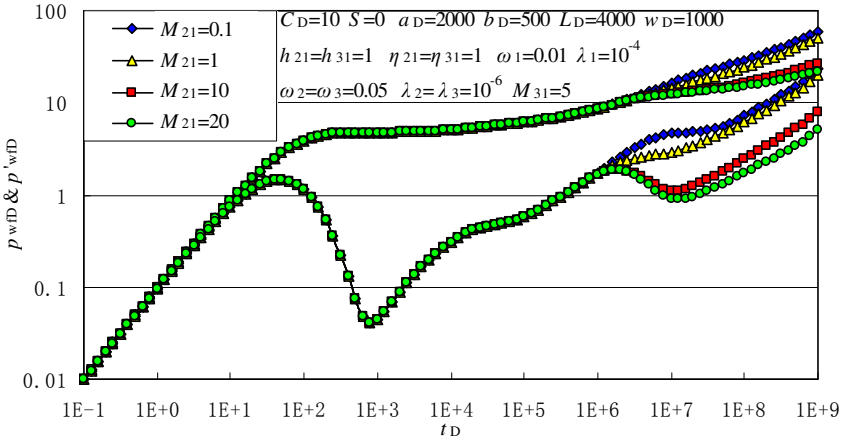

Fig. 5. Effect of mobility ratio on pressure responses for a well in a three-zone linear composite dual-porosity reservoir (M_{21}≠M_{31})

Figs.4 and 5 show the effect of mobility ratio on the pressure responses with other fixed parameters presented in the figure. It can be observed that the effect of mobility ratio is similar to that of thickness ratio. The effect of mobility ratio on type curves becomes obvious once the discontinuity is felt.

For the case the mobility ratio bigger than unit, after the pressure wave reaching the interface, the elevations of dimensionless pressure and pressure derivative curves get lower. That is because a higher mobility ratio means that the outer region is more permeable than the inner region. Thus, the pressure drop is smaller with a same time. The greater the mobility ratio is, the lower the pressure and pressure derivative curves are. In contrast, whereas if the mobility ratio is smaller than unit, after the pressure wave reaching the interface, the elevations of

dimensionless pressure and pressure derivative curves get higher. The smaller the mobility ratio is, the higher the pressure and pressure derivative curves are.

Fig.4 also presents the limiting case that when the mobility of outer region (i.e. region II and III) is small enough, the derivative finally displays a unit slope instead of a 1/2 slope which is the characteristic of a closed system.

Fig. 6 shows the effect of transmissibility ratio on the pressure responses with other fixed parameters presented in the figure. Similar flowing periods can be observed as in Figs.2 and 3. The larger the magnitude of transmissibility ratio, the higher the pressure drop after the discontinuity is felt. That is because when the mobility ratio and thickness ratio are fixed, a higher transmissibility ratio means the product of porosity and the total system compressibility of outer region is smaller than that of the inner region, i.e., the outer region is much less compressible. Thus, the pressure drop is larger with higher transmissibility ratio.

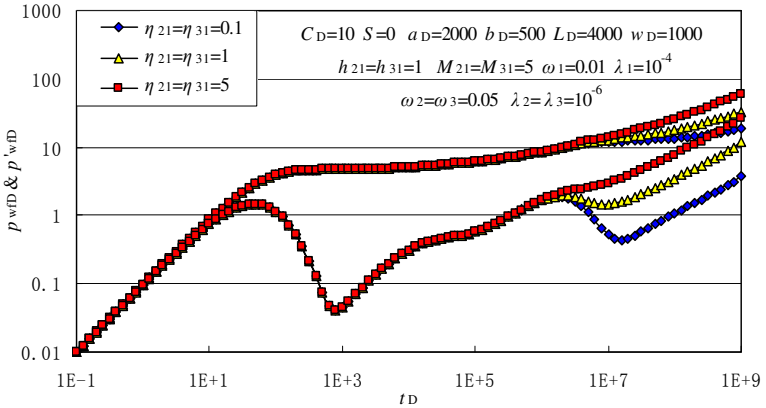

Fig. 6. Effect of transmissibility ratio on pressure responses for a well in a three-zone linear composite dual-porosity reservoir ($\eta_{21}=\eta_{31}$)

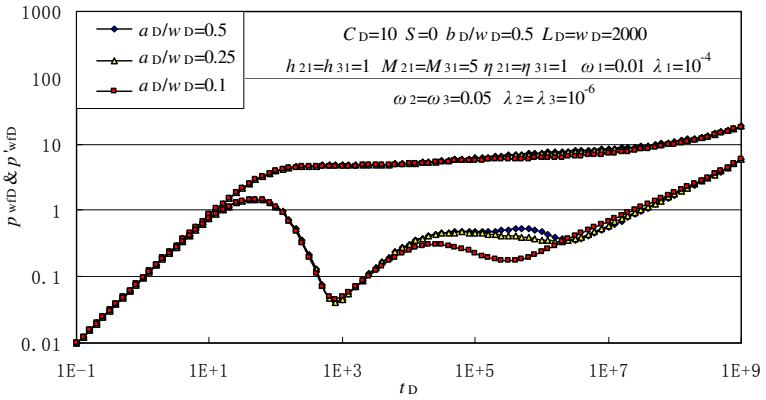

Fig. 7. Effect of well location (a_D) on pressure responses for a well in a three-zone linear composite dual-porosity reservoir

The location of the well in the reservoir is described by two parameters: a_D and b_D. Figs.7 and 8 present the effects of a_D and b_D, respectively, on the pressure transient behavior for a well in a three-zone linear composite dual-porosity reservoir with varied thickness and lateral heterogeneity.

Fig.7 presents the effect of different well locations in the x direction on the pressure transient responses with b_D/w_D=0.5 and L_D=w_D. As shown in Fig.7, wellbore storage period, interporosity flow period and total radial flow period in region I are almost identical for different values of a_D.

For the case of a_D/w_D=0.5, the well is located in the center of region I. The distances between the well and the four boundaries are equal, thus all four boundaries (two parallel impermeable boundaries and two discontinuities) are felt concurrently. After a short transition period, the derivative approached the half-slope line which is characteristic of linear flow in the total system. For a_D/w_D=0.25 and a_D/w_D=0.1, the well is closer to the discontinuity than to the impermeable boundary, so the discontinuity between region I and II is felt first as the departure of derivative from the value of 0.5. Then, the effects of two parallel impermeable boundaries are felt and the discontinuity between region I and III last. At late time, however, all curves approach linear flow behavior illustrated by the half-slope lines on the log-log graphs, irrespective of the magnitude of a_D. That is because when all discontinuities and impermeable boundaries are encountered, the fluid flow in the reservoir depends on the average properties of the linear composite reservoir, so the well location a_D has little effect on the late phase of the pressure responses.

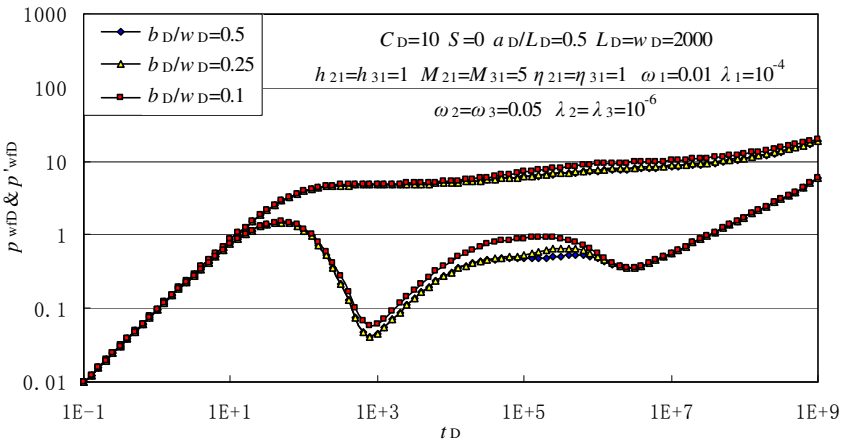

Fig. 8. Effect of well location (b_D) on pressure responses for a well in a three-zone linear composite dual-porosity reservoir

Fig.8 presents the effect of different well locations in the y direction on the pressure transient responses with a_D/L_D=0.5 and L_D=w_D. Again, the departures of the pressure derivative occur whenever one or more boundaries are felt. For example, for the case of a_D/L_D and b_D/w_D both equal to 0.5, two parallel impermeable boundaries and two discontinuities are felt at the same time. The flow in the reservoir is then dominated by the linear flow in the total system. For the case of b_D/w_D=0.25 and b_D/w_D =0.1, the effect of the lower impermeable boundary of the strip reservoir (Fig.1) is felt. At this time, flow in the reservoir is somewhat like that in an infinite reservoir with one fault boundary, thus the pressure derivative double its value to one. The doubling of constant derivative can be observed if the well is closer to one impermeable boundary. Fig.8 also illustrates that the well location b_D has little effect on the late phase of the pressure responses.

6. Conclusions

1. A new analytical solution for the pressure-transient behavior of a line-source well producing at a constant rate in a three-zone, linear composite dual-porosity reservoir is presented in Laplace-Fourier space, which takes into account the changes in reservoir thickness, wellbore storage effect and skin factor. It can easily be inverted to real space, and it is especially useful in predicting pressure performance or analyzing test data from this type of reservoir configuration.
2. Behavior of the solution at the wellbore has been analyzed with help of the pressure derivative. Sensitivity study is done and the effects of relevant parameters, such as thickness ratio, mobility ratio, transmissibility ratio, and the well location, on the pressure transient responses for a well in this type of reservoir are discussed. The late-time linear flow characteristic of strip reservoirs is observed in all curves, irrespective of mobility ratio, thickness ratio, well location or transmissibility ratio.
3. Determination of relevant parameters from the field test data is not straightforward because the pressure response depends on the property contrasts between regions and the location of the well.
4. The mathematical model proposed in this chapter is based on oil reservoir conditions; it is also applicable to gas reservoirs by replacing the pressure term with a pseudo-pressure term.
5. The model proposed in this chapter is for three-zone linear composite dual-porosity reservoirs, but could also be used for analyzing well test data from two-zone linear composite dual-porosity reservoirs.

7. Acknowledgments

This work was supported by National Science Fund for Distinguished Young Scholars of China (Grant No. 51125019), the National Program on Key Basic Research Project (973 Program, Grant No. 2011CB201005) and the Doctoral Fund of Ministry of Education of China (Grant No. 20105121110006).

8. Nomenclature

a = distance between the well and the interface between region I and II

a_D = dimensionless distance between the well and the left interface
b = y coordinate of well location
b_D = dimensionless y coordinate of well location
C_{tf1} = total fracture system compressibility of region I
C_{tf2} = total fracture system compressibility of region II
C_{tf3} = total fracture system compressibility of region III
C_{tm1} = total matrix system compressibility of region I
C_{tm2} = total matrix system compressibility of region II
C_{tm3} = total matrix system compressibility of region III
h_1 = reservoir thickness of region I
h_2 = reservoir thickness of region II
h_3 = reservoir thickness of region III
h_{21} = ratio of thickness of region II to thickness of region I
h_{31} = ratio of thickness of region III to thickness of region I
k_{f1} = fracture permeability of region I
k_{f2} = fracture permeability of region II
k_{f3} = fracture permeability of region III
k_{m1} = matrix permeability of region I
k_{m2} = matrix permeability of region II
k_{m3} = matrix permeability of region III
L = x-extent of region I
m = Fourier variable with respect to y_D
M_{21} =ratio of mobility of region II to mobility of region I
M_{31} =ratio of mobility of region III to mobility of region I
p_{Df1} = dimensionless fracture pressure of region I
p_{Df2} = dimensionless fracture pressure of region II
p_{Df3} = dimensionless fracture pressure of region III
p_{Dm1} = dimensionless matrix pressure of region I
p_{Dm2} = dimensionless matrix pressure of region II
p_{Dm3} = dimensionless matrix pressure of region III
p_{f1} = fracture pressure of region I
p_{f2} = fracture pressure of region II
p_{f3} = fracture pressure of region III
p_{m1} = matrix pressure of region I
p_{m2} = matrix pressure of region II
p_{m3} = matrix pressure of region III
p_i = initial reservoir pressure
q = flow rate at sandface
q_1^* = volumetric flow rate from the matrix system to the fracture system in region I
q_2^* = volumetric flow rate from the matrix system to the fracture system in region II
q_3^* = volumetric flow rate from the matrix system to the fracture system in region III
r_w = wellbore radius
S = skin factor

s = Laplace variable with respect to x_D
t = production time
t_D = dimensionless time
u = Laplace variable with respect to time
v_{f1} = velocity in fracture system of region I
v_{f2} = velocity in fracture system of region II
v_{f3} = velocity in fracture system of region III
w = reservoir width
w_D = dimensionless reservoir width
x = x coordinate of a point
x_D = dimensionless distance in x direction
y = y coordinate of appoint
y_D = dimensionless distance in y direction
α = shape factor
μ = fluid viscosity
ρ_1 = density of fluid in region I
ρ_2 = density of fluid in region II
ρ_3 = density of fluid in region III
ω_1 = storativity ratio of region I
ω_2 = storativity ratio of region II
ω_3 = storativity ratio of region III
λ_1 = interporosity flow coefficient of region I
λ_2 = interporosity flow coefficient of region II
λ_3 = interporosity flow coefficient of region III
ϕ_{f1} = fracture porosity of region I
ϕ_{f2} = fracture porosity of region II
ϕ_{f3} = fracture porosity of region III
ϕ_{m1} = matrix porosity of region I
ϕ_{m2} = matrix porosity of region II
ϕ_{m3} = matrix porosity of region III
δ = delta function denoting the constant-rate line-source well
η_{21} = ratio of transmissibility of region II to transmissibility of region I
η_{31} = ratio of transmissibility of region III to transmissibility of region I
Δp_s = additional pressure drop near the wellbore
p_{wfD} = wellbore pressure drop
$\hat{\bar{p}}^*_{wfD}$ =dimensionless wellbore pressure drop with zero skin and wellbore storage in Laplace-Fourier space
$\hat{\bar{p}}_{wfD}$ = dimensionless wellbore pressure drop incorporating wellbroe storage and skin in Laplace-Fourier space

8.1 Superscripts

¯ = Laplace transformation

^ = Finite Fourier cosine transformation

9. References

Bourdet, D. (2002). *Well Test Analysis: The Use of Advanced Interpretation Models* (First edition), Elsevier Science, ISBN 0-444-50968-2, Amsterdam

Farlow, S.J. (1982). *Partial Differential Equations for Scientists and Engineers*, John Wiley and Sons Inc., ISBN 0-486-97620, New York

Guo, J.C. & Xiang, K.L. (1999) Well Testing Analysis Model and Numerical Solution for a Composite Reservoir with Non-uniform Thickness and Double Media. *Well Testing*, Vol.8, No.1, pp.1-5, ISSN 1004-4388

Han, Y.L.; Huang, B.G.; Wang, N.T. & Wu, Y.M. (2007). Pressure Analysis of Double Porosity Composite Infinite Boundary Reservoir. *Drilling & Production Technology*, Vol.31, No.2, pp.83-85, ISSN 1000-7393

Huang, B.G.; Li, S.C.; Li, X.X. & Wang, N.T. (2002). Solution Analysis of The Bottom Pressure in Dual Porous Composite Reservoir. *Journal of Southwest Petroleum Institute*. Vol.24, No.6, pp. 25-27, ISSN 1674-5086

Huang, L. & Liu, Q.G. (2006). Percolation Mathematic Model in Compound Gas Reservoir with Dual Medium of Excessive Sections. *Well Testing*, Vol.15, No.4, pp.11-14, ISSN 1004-4388

Kikani, J. & Walkup, G.W. (1991). Analysis of Pressure-Transient Tests for Composite Naturally Fractured Reservoirs. *SPEFE*, Vol.6, No.2, pp. 176~182, ISSN 0885-923X

Li, R.Y.; Sun, W.T.; Li, S.C.; Huang, B.G. & Yang, H. (2007). Solution Analysis of Pressure Distribution in Composite Bounded Reservoir with Two Porous Media. *Drilling & Production Technology*. Vol.30, No.1, pp. 54~56, ISSN 1000-7393

Olarewaju J.S. & Lee W.J. (1991). Rate Behavior of Composite Dual-Porosity Reservoirs. *Paper 21703 presented at SPE Production Operations Symposium*, ISBN 978-1-55563-530-5, Oklahoma, 7-9 April 1991

Poon, D.C.C. (1984). Pressure Transient Analysis of a Composite Reservoir with Uniform Fracture Distribution, In: *SPE Paper 13384*, 1984, Availabe from http://www.onepetro.org/mslib/app/Preview.do?paperNumber=00013384&societyCode=SPE

Prado, L.R. & Da Prat, G. (1987). An Analytical Solution for Unsteady Liquid Flow in a Reservoir with a Uniformly Fractured Zone Around the Well. *Paper 16395 presented at SPE Low Permeability Reservoirs Symposium*, ISBN 978-1-55563-595-4, Denver, Colorado, 18-19 May 1987

Satman, A. (1991). Pressure-Transient Analysis of a Composite Naturally Fractured Reservoir. *SPEFE*, Vol.6, No.2, pp.169-175, ISSN 0885-923X

Zhang, L.H.; Guo, J.J. & Liu, Q.G. (2010). A Well Test Model for Stress-Sensitive and Heterogeneous Reservoir with Non-uniform Thickness. *Petroleum Science*, Vol.7, No.4, pp.524-529, ISSN 1625-5107

Zhang, L.H.; Guo, J.J. & Liu, Q.G. (2010). A New Well Test Model for a Two-zone Linear Composite Reservoir with Varied Thicknesses. *Journal of Hydrodynamics*, Vol.22, No.6, pp.804-809, ISBN 1001-6058

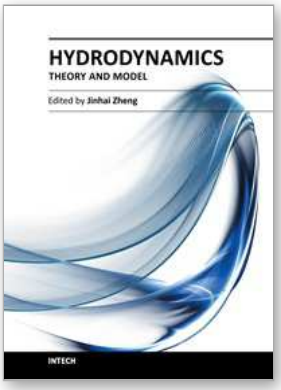

Hydrodynamics - Theory and Model

Edited by Dr. Jin - Hai Zheng

ISBN 978-953-51-0130-7
Hard cover, 306 pages
Publisher InTech
Published online 14, March, 2012
Published in print edition March, 2012

With the amazing advances of scientific research, Hydrodynamics - Theory and Application presents the engineering applications of hydrodynamics from many countries around the world. A wide range of topics are covered in this book, including the theoretical, experimental, and numerical investigations on various subjects related to hydrodynamic problems. The book consists of twelve chapters, each of which is edited separately and deals with a specific topic. The book is intended to be a useful reference to the readers who are working in this field.

INTECH
open science | open minds

InTech Europe
University Campus STeP Ri
Slavka Krautzeka 83/A
51000 Rijeka, Croatia
Phone: +385 (51) 770 447
Fax: +385 (51) 686 166
www.intechopen.com

InTech China
Unit 405, Office Block, Hotel Equatorial Shanghai
No.65, Yan An Road (West), Shanghai, 200040, China
中国上海市延安西路65号上海国际贵都大饭店办公楼405单元
Phone: +86-21-62489820
Fax: +86-21-62489821